AGU PUBLICATIONS

JGR

Journal of Geophysical Research: Space Physics

RESEARCH ARTICLE
10.1002/2015JA022262

Key Points:
- A localized substorm onset current wedge is modulated stepwise
- Buildup of the SCW is due to a dense sequence of arrival of BBFs in the near-Earth tail
- An intense substorm is the result of a group or sequence of more intense and more frequent BBFs

Supporting Information:
- Supporting Information S1
- Movie S1

Correspondence to:
L. Palin,
lpalin@irfu.se

Citation:
Palin, L., et al. (2016), Modulation of the substorm current wedge by bursty bulk flows: 8 September 2002—Revisited, *J. Geophys. Res. Space Physics*, *121*, doi:10.1002/2015JA022262.

Received 11 DEC 2015
Accepted 29 APR 2016
Accepted article online 2 MAY 2016

Modulation of the substorm current wedge by bursty bulk flows: 8 September 2002—Revisited

L. Palin[1], H. J. Opgenoorth[1], K. Ågren[1], T. Zivkovic[1], V. A. Sergeev[3], M. V. Kubyshkina[3], A. Nikolaev[3], K. Kauristie[2], M. van de Kamp[2], O. Amm[2], S. E. Milan[4], S. M. Imber[4], G. Facskó[2,6], M. Palmroth[2], and R. Nakamura[5]

[1]Swedish Institute of Space Physics, Uppsala, Sweden, [2]Finnish Meteorological Institute, Earth Observational Unit, Helsinki, Finland, [3]St. Petersburg State University, Physics Faculty, St. Petersburg, Russia, [4]Department of Physics and Astronomy, University of Leicester, Leicester, UK, [5]Space Research Institute, Austrian Academy of Sciences, Graz, Austria, [6]Geodetic and Geophysical Institute, Research Centre for Astronomy and Earth Sciences, Hungarian Academy of Sciences, Sopron, Hungary

Abstract The ultimate formation mechanism of the substorm current wedge (SCW) remains to date unclear. In this study, we investigate its relationship to plasma flows at substorm onset and throughout the following expansion phase. We revisit the case of 8 September 2002, which has been defined as "one of the best textbook examples of a substorm" because of its excellent coverage by both spacecraft in the magnetotail and ground-based observatories. We found that a dense sequence of arrival of nightside flux transfer events (NFTEs; which can be understood as the lobe magnetic signature due to a bursty bulk flow travelling earthward in the central plasma sheet) in the near-Earth tail leads to a modulation (and further step-like builtup) of the SCW intensity during the substorm expansion phase. In addition, we found that small SCWs are created also during the growth phase of the event in association with another less intense sequence of NFTEs. The differences between the sequence of NFTEs in the growth and expansion phase are discussed. We conclude that the envelope of the magnetic disturbances which we typically refer to as an intense magnetic substorm is the result of a group or sequence of more intense and more frequent NFTEs.

1. Introduction

The original concept of auroral (and later magnetospheric) substorms was introduced by *Akasofu* [1964]. The latest definition of the full substorm concept in various regions of geospace has been given by *Angelopoulos et al.* [2008]: "substorms are global reconfigurations of the magnetosphere involving storage of solar wind energy in the Earth's magnetotail and its abrupt conversion to particle heating and kinetic energy." They are composed of three parts: growth phase (energy loading in the magnetosphere), expansion phase(release of that stored energy), and recovery phase (return of the magnetosphere to its ground state). The mechanism that triggers the substorm onset itself is still unknown even if some models, which try to explain substorms, have been heavily debated. Particularly, current disruption or magnetic reconnection at the near-Earth neutral line (NENL) [*Lui*, 1996; *Baker et al.*, 1996; *Lui*, 2000] have been advocated as alternative explanations for many observed substorm features. Recently, new observations have emphasized the importance of flow bursts in the central plasma sheet, which may trigger the substorm breakup [*Nishimura et al.*, 2010; *Mende et al.*, 2011], also summarized in *Sergeev et al.* [2012].

One of the key signatures of substorms is the localized onset of a three-dimensional current system, generated when the magnetospheric cross-tail current is disrupted and diverted toward the ionosphere by localized field-aligned currents (FACs). This substorm-related 3-D current system, which couples the magnetosphere to the ionosphere, is usually called the substorm current wedge (SCW) [*Atkinson*, 1967; *McPherron et al.*, 1973; *Kepko et al.*, 2014]. It consists of the cross-tail current, a downward FAC at the eastern side of the wedge, an upward FAC at the western side of the wedge, and a connecting westward electrojet in the ionosphere. The magnetic disturbances of this current system on ground level are detectable by ground-based magnetometers at both high [*Opgenoorth*, 1981; *Baumjohann*, 1983] and low latitudes [*McPherron et al.*, 1973]. The method based on low-latitude data is better suited to get the overall current pattern and total intensity rather than the local details, as it is not directly affected by the local ionospheric conductivity conditions (the exact distribution of and the relation between Hall and Pedersen conductances) which determines the high-latitude magnetic disturbances. The SCW is typically very narrow at substorm

onset but expands rapidly to east, west, and poleward during substorm expansion. It is associated with the dipolarization of the magnetic field in the magnetotail, a sign of a global reconfiguration of the magnetosphere, identified as a long-lasting B_z increase in satellite data from that region. Dipolarizations [*Nagai*, 1982] are different from the transient B_z increase associated with localized plasma flows (magnetic pileup associated with local plasma flow), which are called dipolarization fronts (DFs) [*Nakamura et al.*, 2002, 2009; *Lui*, 2014].

The close relationship between plasma sheet flow bursts and the SCW is highlighted in the recent review of *Kepko et al*. [2014], taking advantage of both simulations and observational results. The flows carry plasma with reduced entropy and enhanced magnetic flux that penetrate deep into the magnetosphere [*Panov et al.*, 2010; *Sergeev et al.*, 2014]. The pressure distribution in the inner magnetosphere deflects the flows, thus creating vortices, magnetic shears, and pressure distributions that are associated with field-aligned currents [*Birn et al.*, 1999, 2004; *Keiling et al.*, 2009]. The accumulation of many stopped flow bursts can cause a large-scale pressure buildup responsible for a long-lasting SCW [*Birn and Hesse*, 2014].

Plasma flows brake when entering the inner magnetosphere due to dipolar magnetic field and can "*bounce*" against this magnetic barrier [*Panov et al.*, 2010]. This "bouncing" is observed as a succession of earthward and tailward flow with a decreasing velocity within a few minutes. Due to the oscillatory flow, a "polarization current" and a current associated with the oscillating part of the pressure gradient are created. Those add to the major current wedge generated by the general reconfiguration of the pressure gradient in the magnetotail [*Panov et al.*, 2013]. The same authors also found that those two alternate currents are responsible for the ~2.5 min period modulation of the total ionospheric current that was earlier identified as Pi2 pulsations in ground-based measurements of the magnetic field [*Olson*, 1999, and references therein].

Recently, *Liu et al.* [2015] proposed a new scenario of SCW formation. Using THEMIS mission data they carried out a statistical study of "*wedgelets*," defined as narrow FAC pairs, carried by elemental flux transport units defined as dipolarizing flux bundles (DFBs) [*Liu et al.*, 2013]. Their results show characteristic asymmetries in the individual wedgelets: in the dawn (dusk) sector of the magnetotail, a wedgelet has stronger FAC toward (away from) the Earth than away from (toward) the Earth, so the total net FAC at dawn (dusk) is toward (away from) the Earth. They concluded that the combined effect of many wedgelets is thus the same as that of large-scale region-1-sense SCW, supporting the idea that many small wedgelets comprise the large SCW. They point out that when there are only a few DBFs providing few FACs, a so-called *pseudobreakup* is more likely to occur than a full-scale SCW. The term "*pseudobreakup*" was introduced by *Akasofu* [1964] to describe events with an initial auroral brightening, just like at substorm onset, which, however, subsides a few minutes later without major expansion. If DFBs arrive continuously for several tens of minutes, a long-lasting SCW could thus be sustained by the associated wedgelets. However, a particular weakness of the study by *Liu et al*. [2013] is that it did not consider whether the observed DBFs and wedgelets did, in fact, occur during substorm times or not.

The capability of flow bursts to generate a small current wedge, even under relatively quiet conditions, has recently been investigated by *Palin et al.* [2015]. Using THEMIS data they investigated flow bursts in the magnetotail under quiet solar wind conditions for a period of 7 h preceding a substorm onset. According to the polar cap index (PC index) [*Troshichev et al.*, 1979], this period could be interpreted as a long-lasting growth phase. Eight successive plasma sheet (PS) activations, including DF and bursty bulk flows (BBFs) [*Angelopoulos et al.*, 1992], were observed. When observed from the lobes, these PS activations show the magnetic and particle signatures of earthward contracting recently reconnected flux tubes, i.e., nightside flux transfer events (NFTEs) [*Sergeev et al.*, 1992, 2005]. All PS activations were associated with the formation of a small and localized SCW, as identified in ground-based magnetometer data at auroral and subauroral latitudes. These current wedges appeared to be the direct consequence of BBF arrival in the near tail independently of the amplitude of the DFs. Unfortunately, in the case study of *Palin et al.* [2015], no data were anymore available at the time of the subsequent substorm onset itself or throughout the following substorm expansion phase (neither from spacecraft in the tail nor ground-based instruments).

Sergeev et al. [2005] studied a well-isolated substorm observed by a radial configuration of several spacecraft over central Scandinavia, which they defined as a "textbook example of growth/expansion/recovery phases with unprecedented coverage of all basic regions." During this event two sequences of NFTEs have been identified using magnetic field and particle observations from the Cluster spacecraft. One sequence of

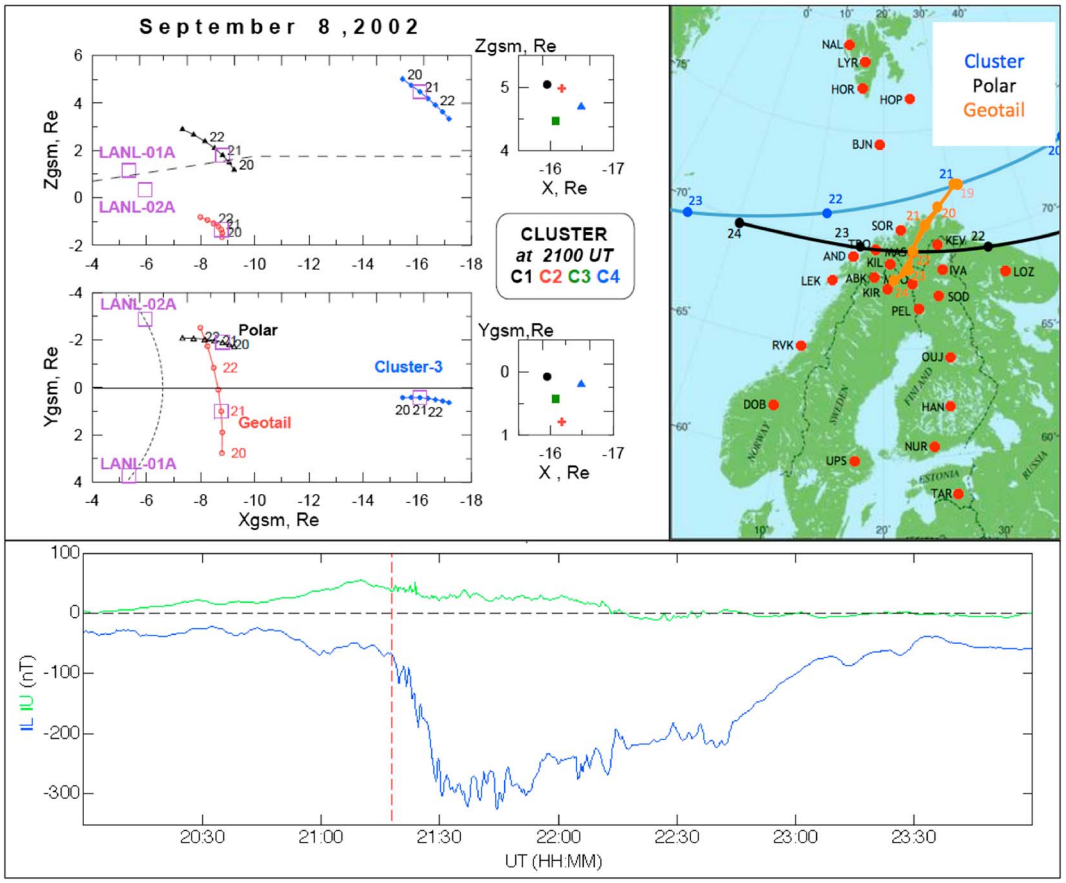

Figure 1. (left) Figure from S05: configuration of basic spacecraft positions on 8 September 2002 in GSM coordinates. The neutral sheet position is indicated on the *X-Z* cross section; spacecraft positions at 21:00 UT are marked by rectangles. (right) Footprints of Cluster, Polar, and Geotail spacecraft obtained from the model by *Tsyganenko* [1989] and location of ground-based magnetometers from the IMAGE network. (bottom) IL and IU indices; red vertical line marks the substorm onset.

NFTEs occurred during the growth phase and the other one at substorm onset and throughout the initial expansion phase. This substorm event study benefits from an exceptionally good coverage by ground-based magnetometers as the footprints of Cluster spacecraft happen to be right above Scandinavia and the International Monitor for Auroral Geomagnetic Effects (IMAGE) magnetometer network at the moment of substorm onset (see Figure 1). Therefore, this particular substorm is of great interest for us, as it will allow us to continue our study of the relation between flow burst and SCW in the substorm expansion phase, which was not possible in the previous case study of *Palin et al.* [2015].

As this is such an exceptionally well instrumented event two other additional papers have already been published on the same period: *Semenov et al.* [2005] and *Keiling et al.* [2006]. *Semenov et al.* [2005] used the data set to test a model of transient time-dependent magnetic reconnection, which is applied to this case study to describe the behavior of NFTEs in the Earth's magnetotail. Using their model they could deduce the location of the reconnection site, which was located at about 29–31 R_E in the magnetotail. *Keiling et al.* [2006] returned to this event to study substorm-related Pi2 pulsations. The series of NFTEs at substorm onset earlier identified by *Sergeev et al.* [2005] (from now on referred to as "S05") has by these authors been interpreted as tail lobe Pi2 pulsations. The first onset of Pi2 pulsation observed on the ground is found to happen only ~30 s after the related observations in the tail. The authors concluded that the Pi2 pulsations both in space and on the ground are, indeed, remotely driven by pulsed magnetic reconnection, explicitly: "reconnection can be coupled to the ionosphere through what is phenomenologically known as Pi2 pulsations."

The aim of this paper is to revisit the observations of S05, using new data analysis methods and additional data provided by a EU-FP7-funded collaborative data analysis project (see below), in order to investigate the relation between flow bursts and SCW in its expansion phase.

2. Instruments

In this study we used magnetic field and particle data from the Cluster mission [*Escoubet et al.*, 2001] provided by the Cluster Active Archive. Spin resolution (4 s) data for the magnetic field were obtained from the FluxGate Magnetometer [*Balogh et al.*, 1997, 2001]. The COmposition and DIstribution Function sensor [*Rème et al.*, 1997, 2001] provided the ion data. We also used the magnetic data from POLAR [*Russell et al.*, 1995] and Geotail [*Kokubun et al.*, 1994] spacecraft, and data from the imaging middle atmosphere geophysical radar (IMAGER) for Magnetopause-to-Aurora Global Exploration (IMAGE) [*Gibson et al.*, 2000].

Ground-based magnetic data are provided by the IMAGE magnetometer network [*Viljanen and Häkkinen*, 1997; *Tanskanen*, 2009]. We like to note that the IMAGE magnetic data are represented in a geographically aligned coordinate system with a north component (*X*), an east component (*Y*), and a vertical *Z* component (positive downward).

For this study we use a particular set of data and models prepared within the EU/FP7-funded research project European CLuster Assimilation Technology (ECLAT) program. ECLAT set out to provide an unparalleled space plasma physics data repository and software tools archive for Solar Terrestrial Physics, built on the existing European Space Agency (ESA) Cluster Active Archive (CAA) initiative. In order to demonstrate the power of the combined space- and ground-based data sets and supporting modeling efforts the program carried out a number of reanalysis attempts of example events, of which this study will serve as an exemplary substorm event study to be included in the CAA along with other ECLAT data sets and models.

3. Observations

3.1. Previously Reported Observations

3.1.1. Interplanetary Magnetic Field Conditions

S05 reported a well-isolated substorm on 8 September 2002, which was preceded by a long period of northward oriented interplanetary magnetic field (IMF), resulting in a cold, dense, and thick plasma sheet preceeding substorm onset. A southward IMF turning occurred at the magnetopause around 20:00 UT, and the IMF turned north again around 21:20 UT. At around 20:30 UT and 21:05 UT, two transient northward turnings of the IMF were observed by ACE and/or Wind (data not shown here).

3.1.2. Substorm Phases

The substorm in question is, in fact, a poststorm substorm (in the late storm recovery phase), but it is well isolated from the storm active phase, both in time and in its disturbance characteristics. It was observed by a radial constellation of spacecraft including Polar and Geotail at $X \sim -9\ R_E$ close to the plasma sheet or plasma sheet boundary layer and Cluster at $X \sim -16\ R_E$ in the lobes at substorm onset. The positions of the spacecraft in the tail are shown in Figure 1, right. Based on ground and tail data S05 found the growth phase to start at 20:15 UT. The substorm onset (expansion phase) was observed at ~21:18 UT in the local time sector 22:00–24:00 magnetic local time (MLT) by both auroral observations of the IMAGE satellite and ground-based magnetometers in Scandinavia. Figure 1, bottom, shows the "IL" and "IU" (image lower and upper) indices, which similarly to the well-known *AL* and *AU* indices are the negative and positive envelope functions of the entire horizontal component magnetic data from the Scandinavian network. A pseudobreakup was identified at 21:06 UT with a weak intensity increase of the westward electrojet, also accompanied by a soft plasma injection to the geostationary orbit (see S05 for detail). According to S05, that pseudobreakup was probably due to either (very localized) ballooning-type instability or due to the braking of a very narrow BBF.

3.1.3. Plasma Sheet Flow Bursts

The term NFTE was introduced by *Sergeev et al.* [1992] to emphasize the similarity between dayside magnetopause flux transfer events (FTEs) and BBFs in the nightside plasma sheet which both involve characteristics of a 3-D propagation of localized reconnected flux tubes. The well-known signature of an NFTE—as observed in the tail lobes—is a very asymmetric bipolar B_z pattern, suggesting an open magnetic structure of the plasma and magnetic field bulge associated with a B_x compression. S05 showed that outside the plasma sheet boundary, the localized bulge-like expansion of the plasma sheet traveling with the flow burst is evidenced by an associated pattern of outward/inward vertical convective flows.

On 8 September 2002, while in the lobes, the Cluster spacecraft encountered multiple cold oxygen ion beams due to ionospheric outflow. A series of negative variations of V_z accompanied by positive B_z variations (Figures 2a–2d, green shadow) suggests an association between plasma tube convection toward the neutral

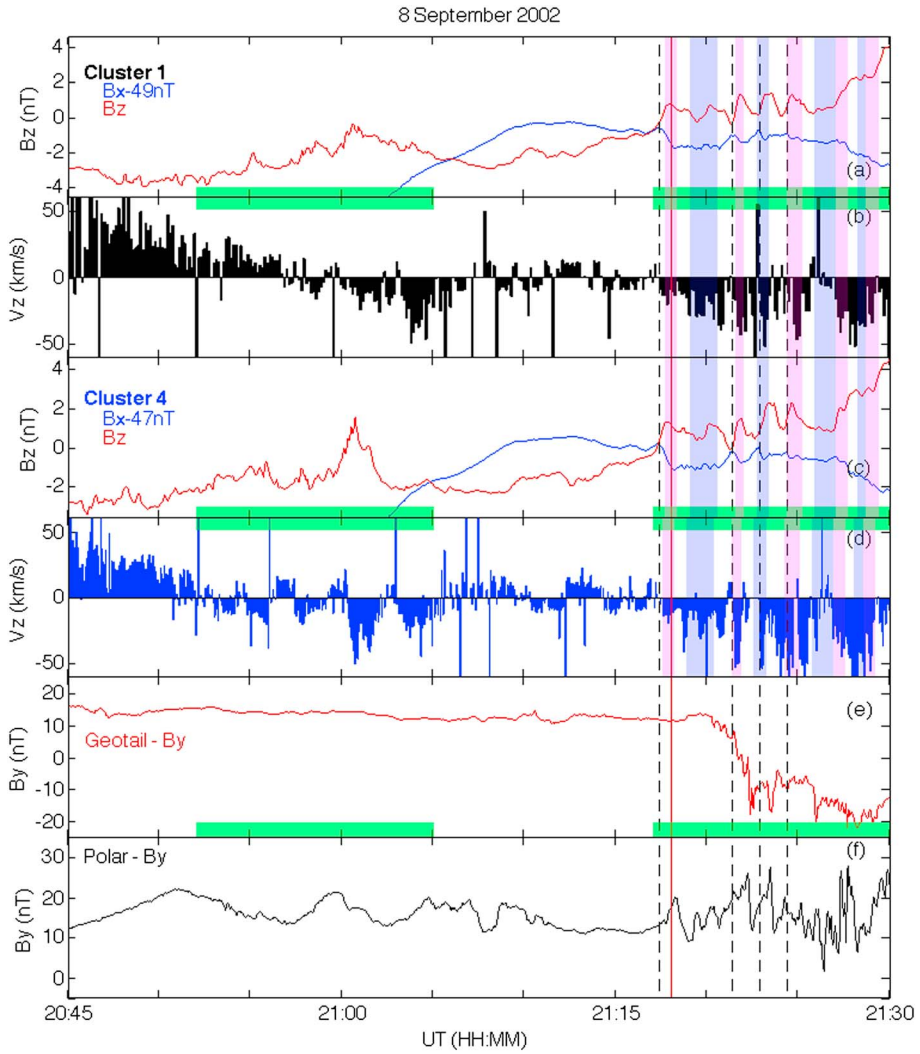

Figure 2. (a and c) B_x (adjusted by a constant offset to be plotted together with B_z) and B_z variations and (b and d) O^+ perpendicular flows at C1 and C4 spacecraft. B_y variations at (e) Geotail and (f) Polar spacecraft. The coordinate system used in this picture is GSM. Green shadows denote the periods of NFTEs identified by S05. Red solid line denotes the substorm expansion phase onset (from S05). Black dashed line denotes the NFTEs around substorm onset, at Cluster (from S05). Pink and blue shadows are explained in text.

sheet and magnetic dipolarization events. S05 note "a systematic phase shift between different components: the V_z and B_z variations anticorrelate each other with little phase shift evident, but the beginning of a positive δB_z (negative δV_z) pulse corresponds to the maximum of B_x variation" (see S05 for details). They interpreted the quarter-period phase shift between the components as "signatures of localized earthward contracting reconnected flux tubes (NFTEs) or flux ropes."

A first sequence of such NFTEs is identified during the growth phase of the substorm, in the time period 20:52–21:05 UT (Figures 2a–2d, green shadow). That these NFTEs are not observed by each Cluster satellite (B_z profile differs especially at C2, not shown here) implies that they are, indeed, small-scale structures traveling in the plasma sheet. A second sequence of NFTEs is identified at substorm onset (around 21:17 UT) and throughout the substorm expansion phase. In that second period, B_z and V_z vary quite similarly at both C1 and C4 (Figure 2), suggesting a relatively large scale of these perturbations during this time. A delay in the magnetic signature from C4 to C1 was pointed out by S05, supporting an earthward propagation of the structures. From the time delay between the probes, their estimation of an earthward propagation of about 500–700 km/s is obtained. The NFTEs identified at substorm onset by S05 are marked by the vertical black dashed lines in Figure 2.

3.2. New Observations Added Through ECLAT Efforts

3.2.1. A Steady Westward Edge of the Aurora

Figure 3 shows the IMAGE satellite data from the proton channel of the spectral imager (SI12, left plot) and the wideband imager (WIC, right plot), which is dominated by electron auroral emissions [*Mende et al*., 2003] depicting the auroral development of the substorm (view from the North Pole). First auroral intensifications are observed in the premidnight sector starting at 20:40 UT, gradually establishing an active auroral oval. According to these images with a 10 min cadence the substorm breakup takes place just before 21:20 (poleward intensification), consistent with the appearance of the substorm onset signatures in the magnetometer and Cluster data above. A particularity of this substorm is that the substorm aurora does not expand to the west, only the east. This is particularly noticeable in the IMAGE FUV/WIC data (right part of Figure 3).

Sergeev et al. [1996a] demonstrated a method (inversion of midlatitude magnetic variations, first introduced by *Horning et al*. [1974]; see *Chu et al*. [2014] for the latest version), in which the global distributions of bay-like perturbations in the magnetic *X* and *Y* components observed at midlatitude stations are fitted to the prediction from a model current system. The model consists of three current systems (symmetric and partial ring currents and the SCW), and particularly, it allows inferring the total SCW current as well as the longitudes of its eastward and westward edges to characterize the spatiotemporal development of substorms. The reconstruction of SCW dynamics based on data from INTERMAGNET (INTErnational Real-time MAGnetic Observatory NETwork; data are available from http://www.intermagnet.org) observations for our substorm is presented in Figure 4, where the simulated locations of the upward (red) and downward (blue) FACs are displayed as a function of time and solar magnetic longitude. As the time step for the INTERMAGNET data is only 1 min, unfortunately, the faster fluctuations seen in the IMAGE data, which we will discuss in the following, cannot be identified in this model data. Thus, we only present the longitudinal development of the substorm current wedge in Figure 4. The westward edge location of the SCW is clearly more or less static (red points on a horizontal line), whereas the eastward edge is expanding eastward (blue points on an increasing curve). Note that the longitudinal expansion of the current wedge appears to occur in steps rather than in a continuous motion. One apparent large step at 21:43 UT is clearly caused by a lack of longitudinal data, but this lies already outside our particular period of interest for this study.

We will later see that the lack of westward expansion quite fortuitously keeps the western substorm edge (and the associated upward field-aligned current features) centered over our Scandinavian network of stations, so we can follow its behavior throughout the expansion phase both by Cluster in the tail and instruments on the ground. During most other substorms such continuous observations are inhibited by rapid substorm expansion out of the field of view of the instruments and spacecraft.

3.2.2. Modulation of the FAC at Substorm Onset

Localized FACs are detectable at high latitudes only indirectly via magnetic field perturbations caused by ionospheric Hall currents encircling the location of the footprint of the FAC, while the actual magnetic disturbances of the field-aligned currents itself below the ionosphere are more or less cancelled by the magnetic effects of the ionospheric Pedersen currents [*Fukushima*, 1971; *Untiedt et al*., 1978; *Opgenoorth et al*., 1980; *Amm and Fujii*, 2008]. A distribution of so-called ionospheric equivalent currents can be reconstructed from ground-based magnetometers. They are "virtual" currents assumed to flow only confined within the ionospheric plane (assumed at 100 km altitude) but causing the same magnetic field change on the ground as the real three-dimensional ionospheric/magnetospheric current system. They are determined using the method of spherical elementary current systems (SECSs) [*Amm and Viljanen*, 1999; *Pulkkinen et al*., 2003]. In these equivalent current maps/patterns a potential footprint of a localized downward (upward) FAC can sometimes be identified by a quasi-circular clockwise (counterclockwise) equivalent current vortex around locations of upward (downward) FAC. The analysis of such equivalent current patterns is, however, often quite difficult, as the magnetic effects of newly superimposed localized field-aligned currents often are hardly visible against the magnetic disturbance of the large-scale growth phase and substorm onset electrojets.

Following *Untiedt et al.* [1978] and *Opgenoorth et al.* [1980, 1983], we therefore use the method of "differential equivalent current vectors" which shows the difference in equivalent currents between the start and end times of selected intervals, which are carefully selected to represent sudden and localized occurrences of new additional current systems. Used effectively, it can be a powerful tool to visualize and understand the magnetic effect of any localized current system added to (or withdrawn from) the preexisting background electrojets. However, the time periods for the differential current patterns have to be carefully selected to

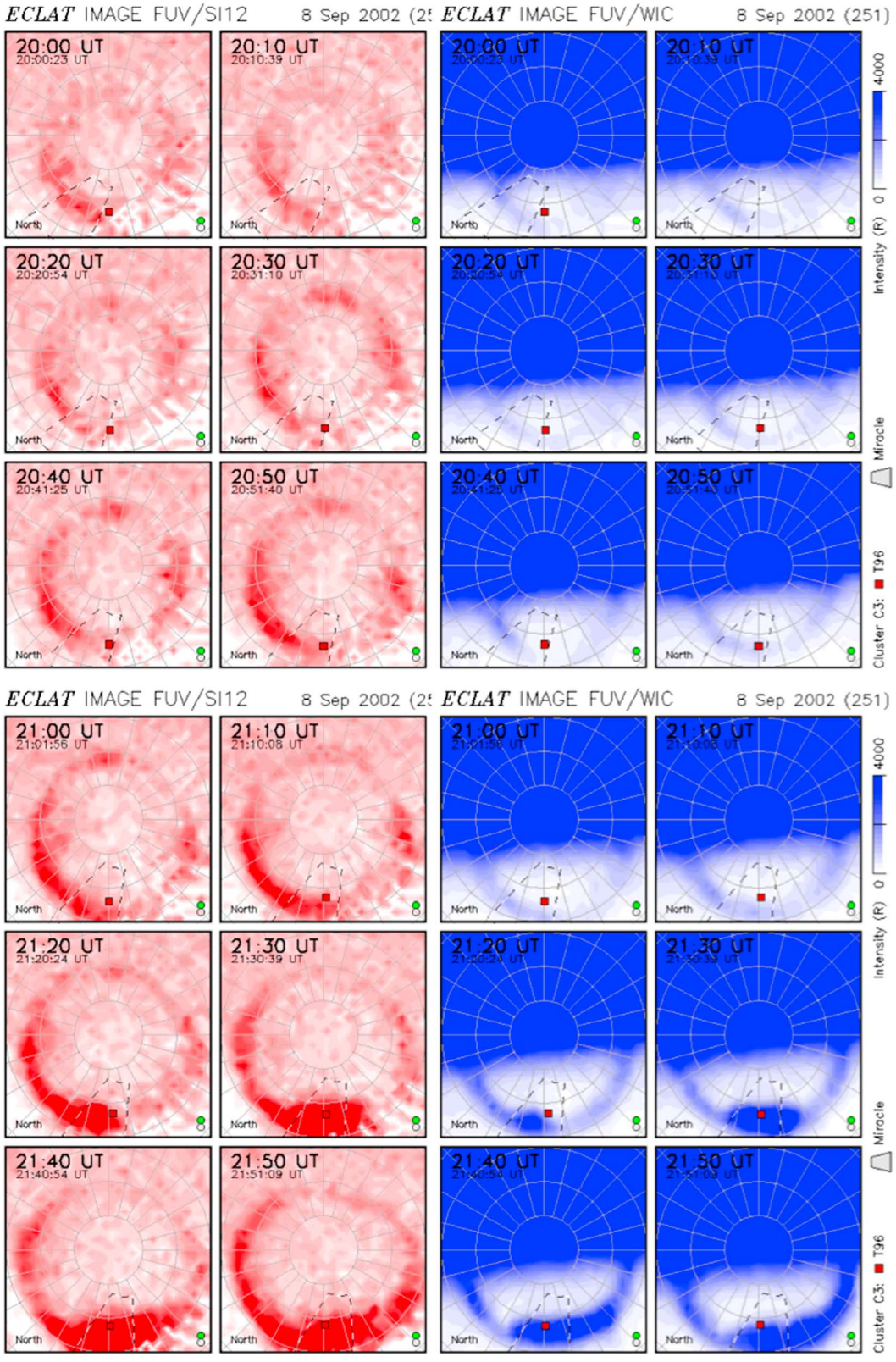

Figure 3. IMAGE satellite global view of the auroral development at two different wavelengths depicting proton aurora (SI12) on the left and wideband emissions from mainly electron aurora on the right (WIC) from 20:00 UT to 22:00 UT. The red square marks the footprint of Cluster 3 location. The area in the dashed lines is the location of MIRACLE network. The two circles at the bottom right of each plot are the quality flags; green means good quality data.

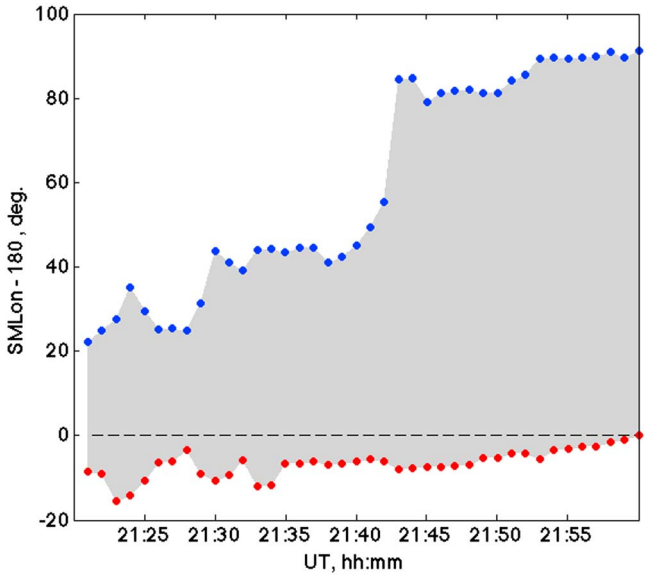

Figure 4. Simulation of the SCW using the model of *Sergeev et al.* [1996a], see text for explanation. T_o is the time of substorm onset in the model. The position of the FAC flowing down (out) to the ionosphere is in blue (red). SMLon is the longitude in the solar magnetic coordinate system.

avoid a mixing of different current systems, which can lead to a completely misleading picture. In this case, for the identification of the differential intervals chosen in Figure 5, we initially inspected the "differential equivalent current patterns" from the original 10 s resolution maps (meaning that each new equivalent current vector was reduced by the current from the preceding map, as to show only the 2-D equivalent current pattern added since the last 10 s). Each 10 s interval which showed a similar pattern as the preceding interval was added to the same integration period (i.e., seen as a continued addition to the same additional pattern on the original background). Only when the next 10 s pattern showed a different or even reverse pattern, the integration was stopped and a new integration period started for as long as the basic new pattern prevailed (and so on). Any motion of the patterns during the integration times would of course lead to a blurring of the final results, but we encountered very little motion of basic patterns during this procedure. Patterns did built up for a certain time and reversed (i.e., decreased) for another period of time. Sometimes new pattern developed slightly shifted from the patterns of previous integration periods, but any such shifts are reflected in the data shown in Figure 5.

Figure 5 shows the resulting differential equivalent currents (black arrows) for such selected (subsequent) intervals during the substorm onset and expansion phase. Clockwise and counterclockwise vortices appear in the black arrow fields. As explained above, these vortices indicate the position of a downward (upward) FAC, marked on the figure by the red (green) circle close to the center of clockwise (counterclockwise) differential equivalent current vortices. As shown in the sketch in Figure 5 (right) the Hall current vortices are not the only noticeable addition in these equivalent current patterns, but often there is an additional westward electrojet; i.e., magnetic effects of the three-dimensional SCW are not completely cancelled. With other words in real life the Pedersen currents are not completely curl free and the Hall currents are not completely divergence free [*Amm et al.*, 2008], depending on the detailed distribution of Hall and Pedersen conductances. This additional westward electrojet superimposed on the Hall current loops results in a shift of the vortex center from west to southwest and east to northeast and a general alignment of the westward current in a southeast-northwest direction [*Opgenoorth et al.*, 1980; *Baumjohann et al.*, 1983].

Thus, the red and green markings are to be understood as the "best estimated location" for the field-aligned current position (be it added or withdrawn current), which is not always at the exact center of the skewed vortex. Another problem with the Scandinavian IMAGE data set is the problem of boundary conditions in the eastern and western, but also north and south directions, as the number of stations outside the IMAGE network fast decreases to a few or none. Any indication of an extra rotation close to a boundary is in the SECS method closed by interpolated vectors outside the confidence area. We have taken great care not to mark any equivalent current vortices which are supported by data from less than three real stations (compare Figures 5 and 1).

From 21:18:30 to 21:25:10 UT, one can see a succession of repeated switch ons and switch offs (or rather partial cancellation) of additional localized current systems in the form of a current wedgelet ("ON" or "OFF" is written in the corresponding panels) with two localized FACs, downward on the eastern edge and upward on the western edge. As of 21:25:10 UT and onward, mainly (only) the westward FAC is observable, because, as previously discussed, the westward edge of the SCW is more or less static above Scandinavia, whereas the eastward edge expands to the east; thus, the downward FAC can be outside the maps in Figure 5. These

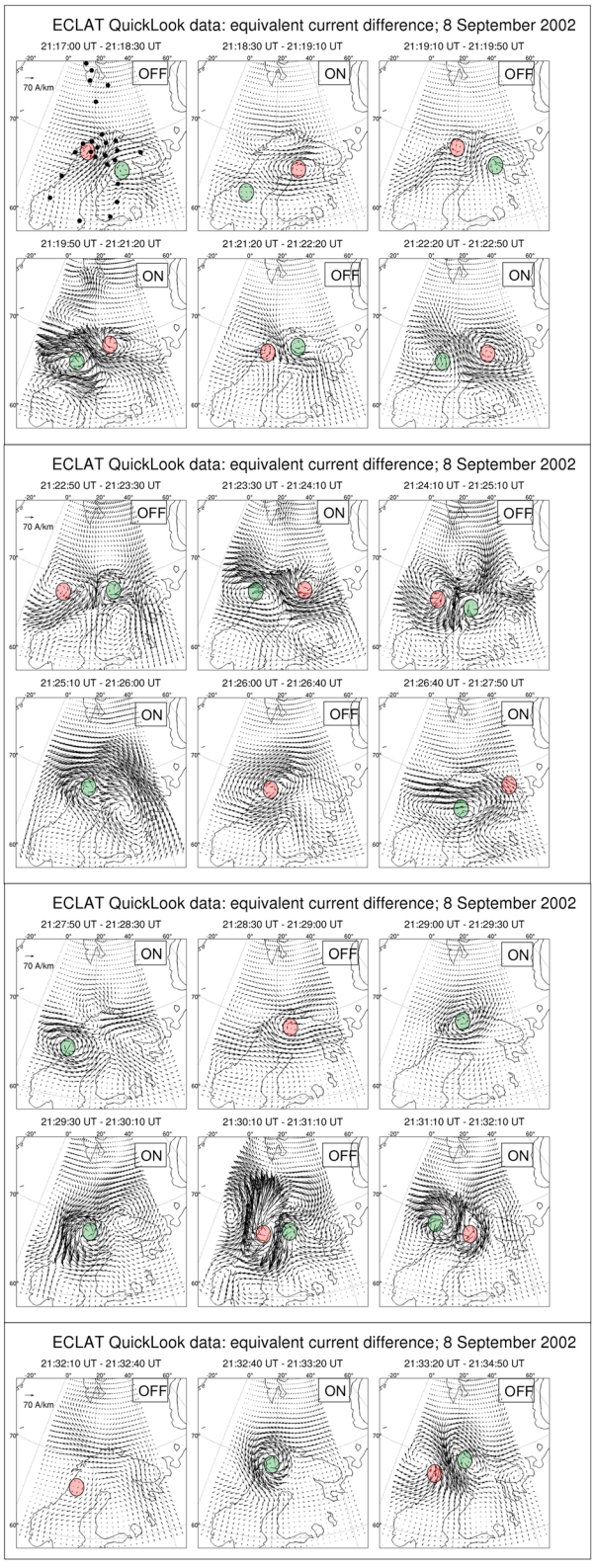

Figure 5. (left) "Differential equivalent current vectors" showing the difference in equivalent currents between the start and end times of selected intervals, i.e., the magnetic effect of any additional current system added to (or withdrawn from) the preexisting large-scale background electrojets. The black dots on the first plot show the location of ground-based magnetometers. Inset on the top right is the sketch of the total equivalent current distribution current distribution when adding a westward electrojet to the circular Hall current patterns encircling the footprints of field-aligned currents (see text).

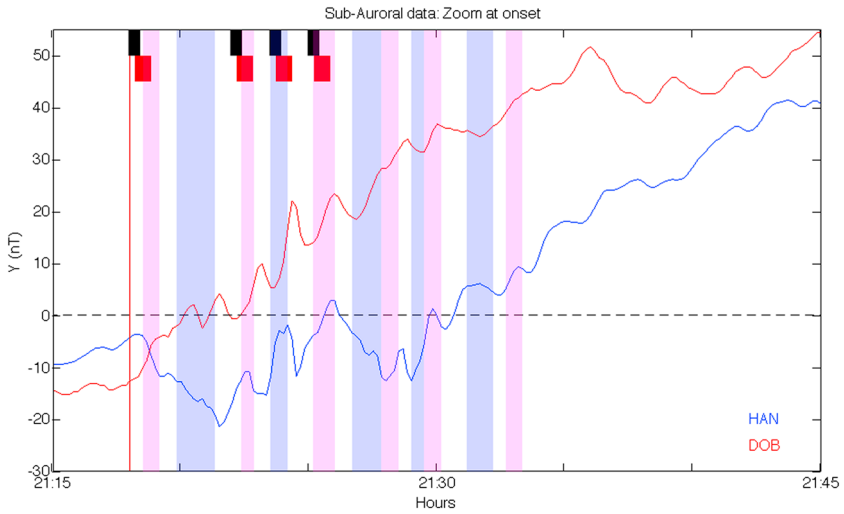

Figure 6. Ground-based magnetometer data from two subauroral stations of the IMAGE magnetometer network—geographic east components of HAN and DOB—around and after substorm onset (for exact station location, see Figure 1). Red solid line is the substorm expansion phase onset (from S05). Pink and blue shadow (two colors used for better visibility of adjacent periods) is the time period where SCW modulation is "ON" in Figure 5. The rectangles on top of the plot mark the expected time period of flow braking in the region from −12 to −9 R_E, assuming a propagation velocity of 700 km/s (black) and 500 km/s (red). See text for detail description.

observational data from the overhead current system are consistent with the simulation of low-latitude data presented in Figure 4. Focusing on the westward part of the three-dimensional current system, the additional upward FAC successively appears and partially disappears, which can be understood as a clear modulation of the gradual builtup of the SCW. Please note that during ON periods we interpret the counterclockwise (clockwise) Hall current vortices as indicators of additional upward (downward) FAC, marked with green and red circles in Figure 5. During OFF periods the corresponding colors are not indicating additional downward (upward) field-aligned currents in an alternating sense, but rather the disappearance of the previous pattern, i.e., a switch off, or at least a partial decrease of the previously appearing SCW onset or SCW modulation.

We like to point out that the identification of the "ON," respectively, "OFF" steps is most clear for the first four or maybe five pulses in the magnetic field data, after which we can still see a similar pattern, but occasional extra vortices do actually sometimes occur adjacent to the main system. In order not to hide this effect we deliberately left one double ON step appear in two separate integration periods (from 21:26:40 to 21:27:50 UT and 21:27:50 to 21:28:30 UT) to show that deterioration of patterns for later pulses (see also 21:25:10–21:26:00 UT for an apparent upward ON loop over Finland, which might instead be the continuation of the downward OFF loop from the previous step, simultaneous with a new upward ON over Norway). We attribute these deficiencies to the fact that only in the very beginning of the pulsed onset one can really assume that the addition and cancellation is on a neutral background conductivity. The longer we move into the process the more remnant pattern must accumulate, blurring the differential vector plots. We also note that the overall character of the NFTEs in the Cluster data is most pronounced for the four pulses, which were already identified by S05.

Another way to search for possible ground signatures of localized field-aligned currents is the more direct method to inspect the magnetograms from selected ground-based stations equatorward from the substorm onset location. Due to curvature and inclination of the magnetic field the magnetic disturbance field from the localized FACs of the SCW can readily be seen in low-latitude magnetometer data (or any magnetometers located sufficiently equatorward from the direct magnetic effect of the circular Hall current loops typically seen at high latitudes, as discussed in the previous section). At lower latitude the FAC wedge is known to create a characteristic direct disturbance field, mainly deflections in the magnetic *H* and *D* components [*McPherron et al.*, 1973]. Upward (downward) FAC induces an increase (decrease) of the *D* component which maximizes at the longitude of the FAC, and the combined current wedge causes an increase in the *H* component, maximizing at the wedge center, at latitudes below the field-aligned magnetospheric current closure paths. Figure 6 shows the IMAGE geographic east component magnetograms (*Y*, which is equivalent to the standard magnetic *D* component) from two subauroral IMAGE stations, one in the west and one in the

east of Scandinavia at the approximate longitudes of the initial substorm current wedge onsets (Dombas (DOB) and Hankasalmi (HAN), respectively). The substorm onset is marked by a red vertical line. At DOB, equatorward of the upward current location, the east component after substorm onset shows an overall increase, which is a signature of the upward FAC. At HAN, equatorward of the initial downward FAC location, the overall tendency after substorm onset is characterized by two successive decreases followed by an increase in the *Y* component. Inspecting Figure 4 we interpret this general trend as a signature of the eastward motion of the eastern edge (downward current) of the SCW. During the beginning of the event it affects HAN by a negative *Y* disturbance, but during the later event HAN is obviously more and more under the influence of the positive *Y* disturbance field of the upward field-aligned current as the downward edge moves toward the east. On top of these general trends which are in agreement with the current direction of the SCW and its subsequent eastward expansion we also note a higher-frequency variation, which is observed in the data from both DOB and HAN. For closer inspection we mark in Figure 6 the time intervals which correspond to an additional Hall current ON as determined from Figure 5. As we have discussed above, we interpret the high-latitude Hall current loops as proxy observations of field-aligned current intensity modulations (switch ON and OFF). The colors are alternating pink or blue, chosen for better visibility of adjacent periods.

For all of these periods, the *Y* component at DOB (red curve) exhibits an increasing, positive pulse, i.e., an increase of upward directed FAC over the longitude of DOB. Interestingly, we see that during the long ON interval at 21:19:50–21:21:20 UT there are two steps in the lower-latitude data, which we actually on second inspection could reconfirm in the 10 s data from the differential equivalent current vectors but which we missed in the first analysis. Similarly, the two adjacent ON events at 21:29:00–21:30:10 (one weak loop and one strong loop in Figure 5) seem to correspond to only one step-like enhancement of the upward field-aligned current in the DOB data.

The *Y* component at HAN (blue curve) is a little more difficult to interpret, mainly due to the superimposed motion of the downward FAC to the east. However, initially we can clearly identify three negative pulses of the *Y* component disturbance field corresponding to enhancements of a downward FAC at the same longitude, when HAN is still clearly under the influence of the modulated downward portion of the SCW. Later in the event, HAN mostly records positive *Y* pulses at the time of the ON modulations of the high-latitude Hall current vortices, which indicates that the upward field-aligned current slightly to the west of HAN has a stronger influence than the downward FAC, which is now further to the east and no longer observed by the IMAGE network.

4. Discussion

4.1. Modulation of the SCW by NFTEs

Based on a statistical analysis, *McPherron et al*. [2011] have shown that plasma flows travel with a constant velocity from $-22\ R_E$ to $-12\ R_E$, then the velocity rapidly decreases to zero from $-12\ R_E$ to $-6\ R_E$. They note that plasma flows are rarely observed inside $-9\ R_E$. S05 derived an earthward propagation velocity of the NFTEs in this event between 500 and 700 km/s. Assuming this velocity to remain constant from the Cluster location to $-12\ R_E$ (respectively, $-9\ R_E$) will give us an estimation of when the flow could start (respectively, stop) its braking phase. The onset time at Cluster of the NFTEs defined by S05 is propagated to $-12\ R_E$ (marked by the leading edge of the bars on the top of Figure 6) and to $-9\ R_E$ (marked by the trailing edge). The black (red) bars correspond to a velocity of 700 km/s (500 km/s). All marks happen to be approximately at the time when an additional current is detected in the ionosphere (black or red bars for each event partially overlapping with either blue or pink color bar in Figure 6). Thus, we conclude that the modulation of the SCW is most likely a direct consequence of the arrival of NFTEs in the near tail. One can also conclude from Figure 6 that the actual velocity of the NFTE is more likely closer to 500 km/s than 700 km/s (producing a slightly better fit of the leading edge of the rectangles).

The first NFTE at substorm onset is, however, quite different from all the other ones in this study because it is associated with a major dipolarization/current disruption. B_z is clearly higher after the NFTE passage than before the NFTE, and B_x is lower after passage than before, which indicates a major energy release at this first substorm onset pulse (see Figures 2a and 2c). Moreover, the decrease in the V_z velocity is far less pronounced than during the passage of the other NFTEs. In Figure 6, the first sign of a SCW is identified by an increase (decrease) of about 10 nT of the east component at DOB (HAN), which is marked by the first pink shadow.

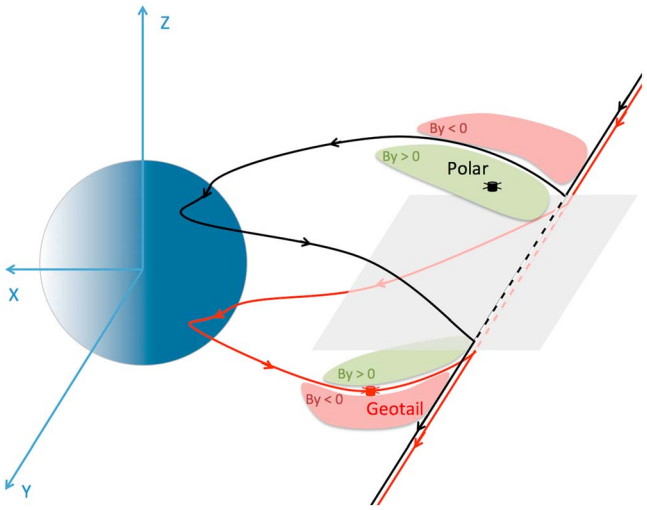

Figure 7. Sketch of the SCW and the position of Polar and Geotail spacecraft relative to the localized FACs in both hemispheres (black north and red south) and on the evening side (upward currents) and morning side (downward currents) of the SCW.

It approximately corresponds to the first NFTE arrival in the near tail. Thus, this first NFTE containing a rather major dipolarization/current disruption is responsible for the initial creation of the SCW.

Assuming a velocity of 500 km/s from the Cluster location to the near tail at about $-12\ R_E$ (where flows are expected to start braking), we can propagate backward the current wedge modulation periods highlighted in Figure 6. The result is shown in Figures 2a–2d. As expected, they match the NFTEs identified by S05, but they also highlight other previously not recognized NFTEs. In each of these periods (pink or blue shadow), an increase of B_z and a decrease of V_z at both Cluster 1 and Cluster 4 (or only one of those spacecraft) are identified.

So far, we have induced the modulation of the substorm current wedge currents by the NFTE sequence from ground-based magnetometer observations at high latitude (Hall current vortices) and subauroral latitudes (direct magnetic field disturbance from FACs.) This has lead us to the relation between NFTEs and FAC onsets as depicted in Figure 2 (top plots) and Figure 6. Fortunately, for this study Polar and Geotail are located at around $-9\ R_E$ in the tail during substorm onset. Polar (Geotail) was in the morning (evening) sector and in the northern (southern) hemisphere during the prime time of interest for this event. During the expansion phase, when NFTEs were observed at Cluster, Polar measures a sequence of positive peaks in the B_y component of the magnetic field (Figure 2f). Near the magnetic equator, the magnetic perturbations induced by the FACs in both hemispheres can cancel each other. As Polar is located slightly above the magnetic equator, the fluctuation in B_y can be interpreted as magnetic effects of downward FAC (from the tail to the ionosphere) located tailward of the Polar spacecraft. This result is consistent with location of the downward field-aligned current in the model study of *Birn and Hesse* [2014]. Geotail, located further away from the magnetic equator thus observing stronger perturbations in B_y than Polar, first observed a weak increase of B_y and then pulses of decreasing B_y (Figure 2e), meaning that it was first earthward and later tailward of the localized upward FAC position. The induced relative positions of the spacecraft with respect to the SCW are shown in Figure 7.

Additionally, so far, we only discussed the pulsed intensification of the substorm current wedge in response to NFTE arrival at the inner edge of the plasma sheet. We note that the first sequence of NFTEs identified by S05 during this event already occurred during the substorm growth phase (first green shadow in Figure 2). The ground-based magnetometers are then located in the evening sector between 22:00 and 24:00 MLT. In analogy to the study by *Palin et al.* [2015] it would be interesting to see whether also in this event the growth phase development is modulated by small-scale current wedgelets. Unfortunately, in this case this is the region where a sharp reversal of the ionospheric convection electric field can be observed, known as the Harang discontinuity (HD) [*Kamide and Vickrey*, 1983; *Kunkel et al.*, 1986; *Heppner*, 1972]. It corresponds to a convection shear zone where the eastward electrojet (equatorward of the shear) and the westward electrojet (poleward of the shear) meet. The HD is typically a source of strong and steady upward FAC. As this event was a poststorm event, the HD was clearly present and already well developed throughout the substorm growth phase. Thus, it would be too complicated to analyze similarly integrated differential equivalent current patterns for the NFTE influence on the growth phase current development (in the same way as we have done for the substorm onset in Figure 5).

Instead, we prepared a movie of the total equivalent ionospheric current over the IMAGE network from 20:00 UT to 21:30 UT which is presented as Movie S1 in supporting information. In that movie, one can see the equivalent currents as black arrows (same as in Figure 5, but now total disturbance vectors, not differential).

The background colors emphasize the areas where current is developing from weak (dark blue ~10 A/km) to strong (dark red ~3000 A/km). The color scale and exact values of the current are very dependent on the baseline definition, which is this case has been taken from a quiet day several days away from the storm period as to derive true values of magnetic disturbances caused by the substorm. Before the substorm onset, several intensifications of the ionospheric current appear as yellow areas (~300 A/km) in different local time (or longitude) regions. The first yellow spot, or noticeable current intensification, is observed in the time period when S05 identified NFTEs in the growth phase. Additionally, Polar observes increases of B_y at in the same time period which might be interpreted as downward FAC. As described previously, these growth phase NFTEs are small-scale structures and may not be observed by all Cluster spacecraft. Thus, we might suspect in analogy of the findings by *Palin et al.* [2015] that the other ionospheric current intensifications during the substorm growth phase could also be triggered by NFTEs, but in a longitudinal different part of the central plasma sheet, which makes them less clearly (or not at all) detectable for the Cluster spacecraft.

In summary, our observations show how NFTE arrival in the near-Earth tail modulates the substorm current wedge, right after substorm onset and throughout the early part of the expansion phase. In addition, we found some evidence that small SCWs are created also during the growth phase of the event in association with another sequence of NFTEs. This has in more detail been shown by *Palin et al.* [2015] for another growth phase situation before a subsequent substorm onset.

4.2. Relation to the Coupled Mode Scenario for the Magnetospheric Dynamics

It is well known that pseudobreakups can occur as substorm precursors [*Koskinen et al.*, 1993] or as isolated events during quiet times [*Sergeev et al.*, 1986] and that they show most of the signatures also found in substorms [*Ohtani et al.*, 1993; *Nakamura et al.*, 1994]. *Nakamura et al.* [1994] already noted that "*the major difference between pseudobreakups and major expansion onsets would be the number of* (…BBF…) *occurrences, as well as the intensity and the scale size of the magnetospheric source*." This view is further supported by the results of *Angelopoulos et al.* [1994] that the occurrence rate of BBF increases from 6% during quiet conditions to 20% during active conditions ("active" defined as *AE*~500 nT). *Sergeev et al.* [1996b] furthermore proposed that "*the initial breakup, the following multiple activations, the pseudobreakups, and other short-term activations during nonsubstorm times are all similar in morphology and have the same formation mechanism*." Thus, they introduced the term impulsive dissipation event (IDE) to describe such elementary units of energy dissipation in the magnetotail. An IDE was defined as a spatially localized process with a time scale as short as ~1 min. According to *Sergeev et al.* [1996b], "*its characteristic features are the activation (or formation) of an auroral arc in the ionosphere and a burst of plasma flow in the nightside plasmasheet*." They further proposed "*two basic magnetospheric processes responsible for energy storage and dissipation during substorms and nonsubstorm times: the global and monotonic quasi-static tail reconfiguration (responsible for the energy storage and partial release during substorm growth phase) and the multiple, local, and sporadic IDEs*." These two modes are supposed to be coupled as it is the evolution of the global mode, which in the end controls the generation of IDEs.

Based on the discussions above we can conclude that our data and analysis presented here for the first time in detail support such general conclusions about the elementary substructure of substorms, which have been presented before by other authors on the basis of less complete data sets. We would like to note further that these general conclusions concerning substorm growth phase and pseudobreakups have already been confirmed by *Palin et al*. [2015] with the first observation of the gradual evolution of the presubstorm ionospheric current disturbance. That study also showed the relation of the number of BBFs involved in each growth phase intensification to the gradual heating of the plasma sheet. At the same time, the global mode is affected by the integrated effects of a sequence of IDEs, thus changing the global configuration of the magnetosphere.

Sergeev et al. [1996b] expressed the opinion that "*an intense substorm is simply a group of more intense and frequent IDEs, rather than a specific entity*." This initial conclusion was based on less complete observations, but it is strongly confirmed by the present study, where more intense and more frequent large-scale NFTEs are observed at substorm onset and throughout substorm expansion phase, leading to the gradual builtup of a complete substorm current wedge. At substorm onset the effects of a sequence of NFTEs are more dramatic and have much larger amplitude as compared to a comparable, but weaker NFTE sequence during the growth phase.

4.3. Additional Understanding Gained from ECLAT Data and Tools

In the following, we will further elaborate how the combined usage of ECLAT tools helped understanding details in this exemplary—but nevertheless complicated—case study. We will show that earlier incomplete, insufficient, or partial data analysis may have given rise to misleading interpretations. Similar errors can certainly be extrapolated to many other substorm studies in the past, which consequently may in many cases have given rise to misconceptions.

4.3.1. Pseudobreakup

The pseudobreakup at 21:06 UT described in S05 was determined using a latitudinal distribution of the westward currents above a meridian near midnight, derived from one latitudinal profile of data from the IMAGE magnetometer network using the 1-D upward continuation method (Figure 4 in S05). As discussed earlier in this manuscript, from full 2-D data of the entire IMAGE network we can deduce that several small SCWs occur throughout the substorm growth phase, albeit at slightly varying central longitudes (and even latitudes). The previously identified pseudobreakup from S05 was merely one of those small SCWs which happened near midnight, but it occurred exactly on the central meridian of the 1-D data analysis, and thus, it clearly stands out in the figure in question. The growth phase is, however, often composed of many of such so-called pseudobreakups, but whether one will find them or not depends on where one looks and which tools are applied to display the data. Only full 2-D data sets can reveal the entire and correct picture.

4.3.2. Pi2 Pulsations

Pi2 pulsations are considered to be a common signature of substorm onset. Their frequency lies between 7 and 25 mHz (40–150 s period).

Keiling et al. [2006] revisited the substorm event of S05 already before us but in terms of understanding magnetic Pi2 pulsations. Using mostly filter techniques on space- and ground-based data and time shifts between the different locations they induced a relation between tail reconnection, NFTEs, fast plasma flows, FAC, and Pi2 pulsations.

Interpreting the NFTEs observed by Cluster as "space Pi2" sources, they [*Keiling et al*., 2006] investigated different scenarios to explain the Pi2 propagation from Cluster location to the ionosphere (ground Pi2). Based on the Cluster data they found an earthward propagation of the NFTEs between 600 and 800 km/s (in agreement with S05). Assuming that a NFTE is associated with a flow burst or BBF in the central plasma sheet, they used an upper limit for the velocity of 1000 km/s to compute a time delay to the near-Earth tail at -9 R_E. Assuming that the flow braking would launch Alfven waves with a velocity of 1000 km/s they found a total time delay of 98 s. However, if the flow breaking instead launches compressional waves with a velocity of 500 km/s, they find a time delay increases to 149 s. According to *Keiling et al*. [2006], both estimated time delays are too long compared to their observations (30 s).

When studying Pi2 pulsations, one typically looks for fast wave propagation, i.e., either magnetosonic waves (propagating perpendicular to field lines) or Alfvén waves (propagating parallel to field lines). Yet in this case study we have shown that NFTEs (signatures of a BBF traveling earthward in the central plasma sheet) occurred exactly at a similarly irregular frequency as typical Pi2 pulsations. When braking in the near tail they will add some currents to the already established SCW. Thus, the added current to the SCW appeared in the same frequency range and the magnetic effect was observed by the ground-based magnetometers. Using simple filtering of data from individual ground-based stations apparent Pi2 pulsations can indeed be observed for extended stretches of time; however, often unexplainable phase shifts are introduced by that method, which even vary from station to station, and change with time. Our alternative explanation of such phase shifts is that the location of the field-aligned current footprints moves through the network of ground-based stations, and thus, any one single station will sooner or later loose synchronization with the two-dimensional magnetic pattern. Our 2-D data in Figure 5 reveal that we are instead dealing with pulses in localized Hall current structures rather than Pi2 pulsations. This can only be resolved with a truly 2-D analysis technique as used in this study.

Also, in accordance with the findings of *Panov et al.* [2013] (presented in the Introduction), here it is the frequency (or rather sporadic periodicity) of the incoming BBFs and not their oscillatory braking which has been (mis)interpreted as Pi2 pulsations.

5. Summary and Conclusions

In this study we use an event defined by S05 as "one of the best textbook examples of a substorm" to investigate in more detail the relationship between NFTEs (or BBFs) and the SCW development during the growth and expansion phase of a substorm. Previous studies have shown that Cluster, located at about $-16\ R_E$ in the lobes, observes two sequences of NFTEs. The large-scale NFTEs have a propagation velocity between 500 and 700 km/s in the expansion phase of the substorm.

The substorm onset happens right above the ground-based IMAGE magnetometer network in Scandinavia and in the close vicinity of field lines connected to several magnetospheric satellite missions. Data show that the westward edge of the SCW is more or less stable above Scandiavia, whereas its eastward part is moving to the east. It means that at substorm onset and throughout the early substorm expansion phase, the modulation of the upward FAC of the SCW can be continuously monitored with the help of an excellent spatial coverage of ground-based instruments and spacecraft.

This study shows that during the substorm growth phase, the NFTE arrival in the near-Earth tail leads to the formation of multiple small SCWs, which is consistent with the findings of *Palin et al.* [2015]. However, the most important finding of this study is that even during the substorm expansion phase, subsequent NFTE arrival in the near-Earth magnetotail leads to a modulation (and further step-like builtup) of the SCW intensity during the expansion phase. Together these intensifications build up the envelope of the magnetic disturbance pattern, which is usually referred to as the "substorm bay" in a typical magnetogram. The first NFTE at substorm onset is associated with a major tail current reduction/disruption, which seems to be responsible for the initial SCW formation, and a first significant global dipolarization of the magnetosphere.

The extraordinary completeness of data for this event has already been utilized in the past for a study of the transition from the growth phase to the expansion phase tail configuration and its plasma characteristics, for the understanding of the pulsating reconnection in the tail and for the understanding of onset-related Pi2 pulsations. In spite of such earlier data evaluations we could show in this study how a more thorough and more complete analysis of all available data and its full content could still lead to basically new results. While some of the relationships identified in this paper have been postulated or shown with less complete data sets (like, e.g., in the paper of *Juusola et al.* [2009]), the clear pulse-like modulation of the SCW in the early expansion phase and its direct relation to the arrival of a sequence of BBFs (NFTEs) in the near-Earth tail has—to the best of our knowledge—never been shown before.

Acknowledgments

Data used in this paper were acquired by satellites operated by ESA (Cluster), NASA (Polar), and JAXA (Geotail). Cluster data were obtained through Cluster Active Archive (CAA) and Geotail data from CDAWEB. We thank C.T. Russell, PI of the MFI instruments at Polar, for providing the high-resolution Polar data. Data from the NASA IMAGE spacecraft (FUV imager) have been provided through the collaboration agreement within the EU/FP7-funded ECLAT project and the University of Leicester, UK. We thank all the institutes who maintain the IMAGE Magnetometer Array within the MIRACLE network (at FMI Helsinki). We thank the INTERMAGNET project for the magnetic observations from their midlatitude stations. L.P. and H.O. acknowledge research funding received from the Swedish National Space Board, and all coauthors acknowledge financial support for the ECLAT project from the EU-FP7 framework program. Even though Olaf Amm (FMI) has not been an official member of the ECLAT team, we felt that the extensive use of his data analysis methods in this paper justified a coauthorship. Due to his sudden and unexpected death in late 2014, in the middle of the finalization of this manuscript, we could no longer offer him that privilege, which is why we decided to honor his valuable contributions by a special dedication of this paper to his memory, and by including him as a posthumous coauthor, which is marked in the author list.

References

Akasofu, S.-I. (1964), The development of the auroral substorm, *Planet. Space Sci.*, *12*, 273–282, doi:10.1016/0032-0633(64)90151-5.

Amm, O., and A. Viljanen (1999), Ionospheric disturbance magnetic field continuation from the ground to the ionosphere using spherical elementary current systems, *Earth Planets Space*, *51*, 431–440, doi:10.1186/BF03352247.

Amm, O., and R. Fujii (2008), Separation of Cowling channel and local closure currents in the vicinity of a substorm breakup spiral, *J. Geophys. Res.*, *113*, A06304, doi:10.1029/2008JA013021.

Angelopoulos, V., et al. (1992), Bursty bulk flows in the inner central plasma sheet, *J. Geophys. Res.*, *97*(A4), 4027–4039, doi:10.1029/91JA02701.

Angelopoulos, V., C. F. Kennel, F. V. Coroniti, R. Pellat, M. G. Kivelson, R. J. Walker, C. T. Russell, W. Baumjohann, W. C. Feldman, and J. T. Gosling (1994), Statistical characteristics of bursty bulk flow events, *J. Geophys. Res.*, *99*, 21,257–21,280, doi:10.1029/94JA01263.

Angelopoulos, V., et al. (2008), Tail reconnection triggering substorm onset, *Science*, *321*, 931, doi:10.1126/science.1160495.

Atkinson, G. (1967), An approximate flow equation for geomagnetic flux tubes and its application to polar substorms, *J. Geophys. Res.*, *72*, 5373–5382, doi:10.1029/JZ072i021p05373.

Baker, D. N., T. I. Pulkkinen, V. Angelopoulos, W. Baumjohann, and R. L. McPherron (1996), Neutral line model of substorms: Past results and present view, *J. Geophys. Res.*, *101*(12), 12,975–13,010, doi:10.1029/95JA03753.

Balogh, A., et al. (1997), The Cluster magnetic fields investigation, *Space Sci. Rev.*, *79*, 65–91, doi:10.1023/A:1004970907748.

Balogh, A., et al. (2001), Overview of in-flight performance and initial results, *Ann. Geophys.*, *19*, 1207–1217, doi:10.5194/angeo-19-1207-2001.

Baumjohann, W. (1983), Ionospheric and field-aligned current systems in the auroral zone: A concise review, *Adv. Space Res.*, *2*, 55–62, doi:10.1016/0273-1177(82)90363-5.

Birn, J., and M. Hesse (2014), The substorm current wedge: Further insights from MHD simulations, *J. Geophys. Res. Solid Earth*, *119*, 3503–3513, doi:10.1002/2014JA019863.

Birn, J., M. Hesse, G. Haerendel, W. Baumjohann, and K. Shiokawa (1999), Flow braking and the substorm current wedge, *J. Geophys. Res.*, *104*, 19,895–19,903, doi:10.1029/1999JA900173.

Birn, J., J. Raeder, Y. L. Wang, R. A. Wolf, and M. Hesse (2004), On the propagation of bubbles in the geomagnetic tail, *Ann. Geophys.*, *22*, 1773, doi:10.5194/angeo-22-1773-2004.

Chu, X., et al. (2014), Development and validation of inversion technique for substorm current wedge using ground magnetic field data, *J. Geophys. Res. Solid Earth*, *119*, 1909–1924, doi:10.1002/2013JA019185.

Escoubet, C. P., M. Fehringer, and M. Goldstein (2001), The Cluster mission, *Ann. Geophys.*, *19*, 1197–1200, doi:10.5194/angeo-19-1197-2001.

Fukushima, N. (1971), Electric current systems for polar substorms and their magnetic effect below and above the ionosphere, *Radio Sci.*, *6*, 269–275, doi:10.1029/RS006i002p00269.
Gibson, W. C., et al. (2000), The IMAGE observatory, *Space Sci. Rev.*, *91*(1–2), 15–50, doi:10.1023/A:1005203207186.
Heppner, J. P. (1972), Electric field variations during substorms: OGO-6 measurements, *Planet. Space Sci.*, *20*(9), 1475–1498, doi:10.1016/0032-0633(72)90052-9.
Horning, B. L., et al. (1974), Application of linear inverse theory to a line current model of substorm current systems, *J. Geophys. Res.*, *79*, 5202–5210, doi:10.1029/JA079i034p05202.
Juusola, L., R. Nakamura, O. Amm, and K. Kauristie (2009), Conjugate ionospheric equivalent currents during bursty bulk flows, *J. Geophys. Res.*, *114*, A04313, doi:10.1029/2008JA013908.
Kamide, Y., and J. F. Vickrey (1983), Variability of the Harang discontinuity as observed by the Chatanika radar and the IMS Alaska magnetometer chain, *Geophys. Res. Lett.*, *10*, 159–162, doi:10.1029/GL010i002p00159.
Keiling, A., et al. (2006), Association of Pi2 pulsations and pulsed reconnection: ground and Cluster observations in the tail lobe at 16 R_E, *Ann. Geophys.*, *24*, 3433–3449, doi:10.5194/angeo-24-3433-2006.
Keiling, A., et al. (2009), Substorm current wedge driven by plasma flow vortices: THEMIS observations, *J. Geophys. Res.*, *114*, A00C22, doi:10.1029/2009JA014114.
Kepko, L., R. L. McPherron, O. Amm, S. Apatenkov, W. Baumjohann, J. Birn, M. Lester, R. Nakamura, T. I. Pulkkinen, and V. Sergeev (2014), Substorm current wedge revisited, *Space Sci. Rev.*, 1–46, doi:10.1007/s11214-014-0124-9.
Kokubun, S., T. Yamamoto, M. H. Acuna, K. Hayashi, K. Shiokawa, and H. Kawano (1994), The Geotail magnetic field experiment, *J. Geomag. Geoelectr.*, *46*, 7–21, doi:10.5636/jgg.46.7.
Koskinen, H. E. J., R. E. Lopez, R. J. Pellinen, T. I. Pulkkinen, D. N. Baker, and T. Bösinger (1993), Pseudobreakups and substorm growth phase in the ionosphere and magnetosphere, *J. Geophys. Res.*, *98*, 5801–5813, doi:10.1029/92JA02482.
Kunkel, T., W. Baumjohann, J. Untiedt, and R. Greenwald (1986), Electric fields and currents at the Harang discontinuity: A case study, *J. Geophys.*, *59*, 73–86.
Liu, J., V. Angelopoulos, A. Runov, and X.-Z. Zhou (2013), On the current sheets surrounding dipolarizing flux bundles in the magnetotail: The case for wedgelets, *J. Geophys. Res. Solid Earth*, *118*, 2000–2020, doi:10.1002/jgra.50092.
Liu, J., V. Angelopoulos, X.-Z. Zhou, Z.-H. Yao, and A. Runov (2015), Cross-tail expansion of dipolarizing flux bundles, *J. Geophys. Res. Solid Earth*, *120*, 2516–2530, doi:10.1002/2015JA020997.
Lui, A. T. Y. (1996), Current disruption in the Earth's magnetosphere: Observations and models, *J. Geophys. Res.*, *101*, 13,067–13,088, doi:10.1029/96JA00079.
Lui, A. T. Y. (2014), Evidence for two types of dipolarization in the Earth's magnetotail, *J. Atmos. Sol. Terr. Phys.*, *115*, 17–24, doi:10.1016/j.jastp.2013.10.002.
Lui, A. T. Y. (2000), Tutorial on geomagnetic storms and substorms, *IEEE Trans. Plasma Sci.*, *28*(6), 1854–1866, doi:10.1109/27.902214
McPherron, R. L., C. T. Russell, and M. P. Aubry (1973), Satellite studies of magnetospheric substorms on August 15, 1968: 1. State of the magnetosphere, *J. Geophys. Res.*, *78*(16), 3044–3053, doi:10.1029/JA078i016p03044.
McPherron, R. L., T.-S. Hsu, J. Kissinger, X. Chu, and V. Angelopoulos (2011), Characteristics of plasma flows at the inner edge of the plasma sheet, *J. Geophys. Res.*, *116*, A00I33, doi:10.1029/2010JA015923.
Mende, S. B., H. U. Frey, V. Angelopoulos, and Y. Nishimura (2011), Substorm triggering by poleward boundary intensification and related equatorward propagation, *J. Geophys. Res.*, *116*, A00I31, doi:10.1029/2010JA015733.
Mende, S. B., H. U. Frey, T. J. Immel, J.-C. Gerard, B. Hubert, and S. A. Fuselier (2003), Global Imaging of Proton and Electron Aurorae in the far Ultraviolet, *Space Sci. Rev.*, *109*, 211–254, doi:10.1023/B:SPAC.0000007520.23689.08.
Nagai, T. (1982), Observed magnetic substorm signatures at synchronous altitude, *J. Geophys. Res.*, *87*, 4405–4417, doi:10.1029/JA087iA06p04405.
Nakamura, R., D. N. Baker, T. Yamamoto, R. D. Belian, E. A. Bering III, J. R. Benbrook, and J. R. Theall (1994), Particle and field signatures during pseudobreakup and major expansion onset, *J. Geophys. Res.*, *99*, 207–221, doi:10.1029/93JA02207.
Nakamura, R., et al. (2002), Motion of the dipolarization front during a flow burst event observed by Cluster, *Geophys. Res. Lett.*, *29*(20), 1942, doi:10.1029/2002GL015763.
Nakamura, R., et al. (2009), Evolution of dipolarization in the near-Earth current sheet induced by earthward rapid flux transport, *Ann. Geophys.*, *27*, 1743–1754, doi:10.5194/angeo-27-1743-2009.
Nishimura, Y., L. Lyons, S. Zou, V. Angelopoulos, and S. Mende (2010), Substorm triggering by new plasma intrusion: THEMIS all-sky imager observations, *J. Geophys. Res.*, *115*, A07222, doi:10.1029/2009JA015166.
Ohtani, S., et al. (1993), A multisatellite study of a pseudo-substorm onset in the near-Earth magnetotail, *J. Geophys. Res.*, *98*, 19,355–19,367, doi:10.1029/93JA01421.
Olson, J. V. (1999), Pi2 pulsations and substorm onsets: A review, *J. Geophys. Res.*, *104*(A8), 17,499–17,520, doi:10.1029/1999JA900086.
Opgenoorth, H. J. (1981), Current systems associated with small scale auroral structures, in *Suomalainen Tiedeakatemia The Finn.-Am. Auroral Workshop*, edited by L. Jalonen and T. Nygren.
Opgenoorth, H. J., R. J. Pellinen, K. U. Kaila, H. Maurer, F. Kueppers, W. J. Heikkila, and P. Tanskanen (1980), Ground-based observations of an onset of localized field-aligned currents during auroral breakup around magnetic midnight, *J. Geophys. Z. Geophys.*, *48*, 101–115.
Opgenoorth, H. J., R. J. Pellinen, W. Baumjohann, E. Nielsen, G. Marklund, and L. Eliasson (1983), Three-dimensional current flow and particle precipitation in a westward travelling surge (observed during the Barium-Geos Rocket Experiment), *J. Geophys. Res.*, *88*(A4), 3138–3152, doi:10.1029/JA088iA04p03138.
Palin, L., et al. (2015), Three-dimensional current systems and ionospheric effects associated with small dipolarization fronts, *J. Geophys. Res. Solid Earth*, *120*, 3739–3757, doi:10.1002/2015JA021040.
Panov, E. V., et al. (2010), Multiple overshoot and rebound of a bursty bulk flow, *Geophys. Res. Lett.*, *37* L08103, doi:10.1029/2009GL041971.
Panov, E. V., W. Baumjohann, R. Nakamura, O. Amm, M. V. Kubyshkina, K.-H. Glassmeier, J. M. Weygand, V. Angelopoulos, A. A. Petrukovich, and V. A. Sergeev (2013), Ionospheric response to oscillatory flow braking in the magnetotail, *J. Geophys. Res. Solid Earth*, *118*, 1529–1544, doi:10.1002/jgra.50190.
Pulkkinen, A., O. Amm, A. Viljanen, and B. E. A. R. Working Group (2003), Ionospheric equivalent current distributions determined with the method of spherical elementary current systems, *J. Geophys. Res.*, *108*(A2), 1053, doi:10.1029/2001JA005085.
Rème, H., et al. (1997), The Cluster Ion Spectrometry (CIS) experiment, *Space Sci. Rev.*, *79*, 303–350, doi:10.1023/A:1004929816409.
Rème, H., et al. (2001), First multispacecraft ion measurements in and near the Earth's magnetosphere with the identical Cluster Ion Spectrometry (CIS) experiment, *Ann. Geophys.*, *19*, 1303–1354, doi:10.5194/angeo-19-1303-2001.

Russell, C. T., R. C. Snare, J. D. Means, D. Pierce, D. Dearborn, M. Larson, G. Barr, and G. Le (1995), The GGS/Polar magnetic field investigation, *Space Sci. Rev.*, *71*, 563–582, doi:10.1007/BF00751341.

Semenov, V. S., T. Penz, V. V. Ivanova, V. A. Sergeev, H. K. Biernat, R. Nakamura, M. F. Heyn, I. V. Kubyshkin, and I. B. Ivanov (2005), Reconstruction of the reconnection rate from Cluster measurements: First results, *J. Geophys. Res.*, *110*, A11217, doi:10.1029/2005JA011181.

Sergeev, V. A., A. G. Yahnin, R. A. Rakhmatulin, S. I. Solovjev, F. S. Mozer, D. J. Williams, and C. T. Russell (1986), Permanent flare activity in the auroral zone, *Planet. Space Sci.*, *34*, 1169–1188, doi:10.1016/0032-0633(86)90055-3.

Sergeev, V. A., L. I. Vagina, R. D. Elphinstone, J. S. Murphree, D. J. Hearn, L. L. Cogger, and M. L. Johnson (1996a), Comparison of UV optical signatures with the substorm current wedge as predicted by an inversion algorithm, *J. Geophys. Res.*, *101*, 2615–2627, doi:10.1029/95JA00537.

Sergeev, V. A., T. I. Pulkkinen, and R. J. Pellinen (1996b), Coupled-mode scenario for the magnetospheric dynamics, *J. Geophys. Res.*, *101*(A6), 13,047–13,065, doi:10.1029/95JA03192.

Sergeev, V. A., et al. (2005), Transition from substorm growth to substorm expansion phase as observed with a radial configuration of ISTP and Cluster spacecraft, *Ann. Geophys.*, *23*, 2183–2198, doi:10.5194/angeo-23-2183-2005.

Sergeev, V. A., V. Angelopoulos, and R. Nakamura (2012), Recent advances in understanding substorm dynamics, *Geophys. Res. Lett.*, *39*, L05101, doi:10.1029/2012GL050859.

Sergeev, V. A., I. A. Chernyaev, V. Angelopoulos, A. V. Runov, and R. Nakamura (2014), Stopping flow bursts and their role in the generation of the substorm current wedge, *Geophys. Res. Lett.*, *41*, 1106–1112, doi:10.1002/2014GL059309.

Sergeev, V., R. C. Elphic, F. S. Mozer, A. Saint-Marc, and J.-A. Sauvaud (1992), A two-satellite study of nightside flux transfer events in the plasma sheet, *Planet. Space Sci.*, *40*, 1551–1572, doi:10.1016/0032-0633(92)90052-P.

Tanskanen, E. I. (2009), A comprehensive high-throughput analysis of substorms observed by IMAGE magnetometer network: Years 1993–2003 examined, *J. Geophys. Res.*, *114*, A05204, doi:10.1029/2008JA013682.

Troshichev, O. A., B. M. Kuznetsov, and N. P. Dmitrieva (1979), Polar cap magnetic activity as a signature of substorm development, *Planet. Space Sci.*, *27*, 217–221, doi:10.1016/0032-0633(79)90063-1.

Tsyganenko, N. A. (1989), A magnetospheric magnetic field model with a warped tail current sheet, *Planet. Space Sci.*, *37*, 5–20, doi:10.1016/0032-0633(89)90066-4.

Untiedt, J., R. Pellinen, F. Küppers, H. J. Opgenoorth, W. D. Pelster, W. Baumjohann, H. Ranta, P. Kangas, P. Czechowsky, and W. J. Heikkila (1978), Observations of the initial development of an auroral and magnetic substorm at magnetic midnight, *J. Geophys.*, *45*, 41–56.

Viljanen, A., and L. Häkkinen (1997), IMAGE magnetometer network, in *Satellite-Ground Based Coordination Sourcebook*, *Eur. Space Agency Spec. Publ.*, ESA-SP1198, edited by M. Lockwood, M. N. Wild, and H. J. Opgenoorth, pp. 111–117.